Triggered and recurrent slow slip in North Sulawesi, Indonesia

Nijholt, N.; Simons, W.; Riva, R.; Efendi, J.; Sarsito, D.; Broerse, T.

DOI
10.1016/j.tecto.2024.230416

Publication date
2024

Document Version
Final published version

Published in
Tectonophysics

Tectonophysics 885 (2024) 230416

Contents lists available at ScienceDirect

Tectonophysics

journal homepage: www.elsevier.com/locate/tecto

Triggered and recurrent slow slip in North Sulawesi, Indonesia

N. Nijholt [a,e,*], W. Simons [a], R. Riva [b], J. Efendi [c], D. Sarsito [d], T. Broerse [b,e]

[a] Department of Space Engineering, Faculty of Aerospace Engineering, Delft University of Technology, Delft, the Netherlands
[b] Department of Geoscience and Remote Sensing, Faculty of Civil Engineering and Geosciences, Delft University of Technology, Delft, the Netherlands
[c] BIG (Badan Informasi Geospasial/Geospatial Information Agency), Java, Indonesia
[d] Faculty of Earth Sciences and Technology, ITB (Institut Teknologi Bandung/Institute of Technology Bandung), Geodesy Research Group, Bandung, Indonesia
[e] Department of Earth Sciences, Utrecht University, Utrecht, the Netherlands

ARTICLE INFO

Keywords:
Slow slip event
Sulawesi
Transient surface motion
Fault interaction
GNSS observations

ABSTRACT

Nearby faults interact with each other through the exchange of stress. However, the extent of fault interaction is poorly understood. In particular, interactions may lead to slow-slip activity, resulting in episodes of transient surface motion. Our study concentrates on Northwest Sulawesi (Indonesia), which hosts two fault zones with potential for major earthquakes and tsunamis: the strike-slip Palu-Koro fault and the Minahassa subduction zone. Thanks to a 20-year-long effort in geodetic monitoring, we are able to identify multiple periods during which surface velocities deviate from their interseismic trend. We use a Bayesian methodology with forward predictions of slip on the two fault interfaces to match the observations following the 2018 M_w7.5 Palu earthquake, and infer that both deep afterslip on the Palu-Koro fault and slow slip on the Minahassa subduction interface have caused the observed transient surface motion. This finding represents the first recording of a slow slip event on the Minahassa subduction interface. We also infer that the subduction interface and the strike-slip fault are likely interacting on a regular basis.

1. Introduction

At Northwest Sulawesi, the Minahassa subduction zone runs east-west offshore the North Arm and meets the Palu-Koro fault at its western termination (Fig. 1). Several tsunamigenic earthquakes struck the island of Sulawesi, Indonesia, over the past 30 years; the largest recorded event occurred at the Minahassa slab interface, in 1996 (Fig. 1; Pelinovsky et al. (1997)), with a M_w 7.9. The left-lateral Palu-Koro fault recently hosted a devastating M_w 7.5 event through a shallow rupture over multiple fault segments (Socquet et al., 2019; Simons et al., 2022). Over the past three decades, the GNSS network on Sulawesi has gradually been densified (Simons et al., 2022). The geodetic network confirms the presence of 4 $cmyr^{-1}$ of relative motion accommodated at both the Palu-Koro fault and the Minahassa subduction zone (Socquet et al., 2006). A view on locking patterns along the slab interface is still absent due to the limited spatial coverage of geodetic observations. Hence, to this day there is no clear evidence to which degree slip deficit accumulates along the Minahassa plate interface. The relative lack of major earthquakes at the Minahassa subduction zone over the past decades, except for the 1996 M_w7.9 and 2008 M_w7.4 events (Fig. 1 A), offers the possibility that episodic aseismic slip accommodates a significant part of the converging motion.

Per definition, seismogenic faults slip transiently. The slip deficit that is accumulated through locked patches on fault interfaces can be distributed over prolonged periods of time (Hirose et al., 1999; Dragert et al., 2001), as opposed to the sudden release of elastic energy through fast slip as earthquakes. Transient (potentially aseismic) slip is usually named afterslip when successive to a major earthquake on the same seismic interface as it is triggered by the co-seismic stress perturbation (e.g., Marone et al., 1991). If transient slip does not directly follow an earthquake, it is called a slow-slip event (SSE). Like earthquakes, SSEs have been detected in GNSS time series for sites overlying subducting plate interfaces and nearby major strike-slip faults worldwide (e.g., Obara and Kato, 2016). Several types of SSEs can be distinguished based on their temporal fingerprint and type of observation (e.g., Beroza and Ide, 2011; Obara and Kato, 2016). SSEs can occur up- and down-dip as well as along-strike of locked patches in seismogenic zones (Hirose et al., 1999; Obara et al., 2004; Ishihara, 2003), they can last from hours to a couple of days to many months (Ishihara, 2003; Obara et al., 2004; Hirose et al., 1999) and their equivalent moment magnitude that is resolvable by geodetic measurements varies roughly between M_w4.5 and 7.5 (e.g., Ide et al., 2007a, 2007b; Beroza and Ide, 2011; Obara and Kato,

* Corresponding author at: Department of Earth Sciences, Utrecht University, Utrecht, the Netherlands.
E-mail addresses: n.nijholt-2@tudelft.nl, n.nijholt@uu.nl (N. Nijholt).

https://doi.org/10.1016/j.tecto.2024.230416
Received 6 September 2023; Received in revised form 24 June 2024; Accepted 4 July 2024
Available online 6 July 2024

2016). The contribution of SSEs to the long-term slip budget also varies per region; SSEs hold a major contribution for the subduction interfaces at Hikurangi (Wallace and Beavan, 2010) and the Guerrero Gap (Radiguet et al., 2012) where SSEs occur on wide extents of the shallow subduction interface. On other subduction interfaces, such as the Nankai (Takagi et al., 2019) and Cascadia subduction zones (Bartlow, 2020), SSEs occur in specific depth ranges whilst most of the shallow subduction interface remains mostly locked, i.e., the SSEs have a smaller contribution to the overall slip budget on the interface. Assessing the seismogenic potential of a subduction interface is therefore reliant on the determination of SSE activity. In this it is important to note that SSEs can either relieve or increase stress on the same subduction interface (Segall and Bradley, 2012; Voss et al., 2018; Cruz-Atienza et al., 2021). For the Minahassa subduction interface no SSEs have been detected in the past.

Another important factor for the seismic hazard of a region is the potential for fault interactions. Namely, slip on one fault can trigger activity on another fault through either dynamic (e.g., Miyazawa and Mori, 2005) or static stress changes (e.g., Toda et al., 1998). SSEs (can) influence the seismogenic potential of fault interfaces by activity on other major faults in the direct vicinity of the SSE host (e.g., Saltogianni et al., 2021). Such fault interactions are reported only sparsely, with evidence of both triggering (Hamling and Wallace, 2015) and delaying (Wallace et al., 2014) motion reciprocally. The SSE on the Hikurangi subduction interface triggered by the complex Kaikōura earthquake which had a large component of shallow crustal activity (Wallace et al., 2018; Wei et al., 2018) highlights the triggering potential of crustal scale faults. The triggering of an SSE also outlines potential earthquake sources as SSEs are found to surround mega-thrust patches that are locked (Obara and Kato, 2016). More observations of fault interactions and their (slow) slip events are needed to better ascertain the imminent seismogenic and tsunamigenic potential of these faults.

Previous studies suggested that the island of Sulawesi holds such a setting where major, seismogenic faults interact (Walpersdorf et al., 1998; Vigny et al., 2002). We assess whether observable interaction between the Palu-Koro fault and the Minahassa subduction interface takes place using an extensive dataset that also includes displacements due to the 2018 M_w7.5 Palu earthquake. Nijholt et al. (2021) report transient deformation near Palu in the 11 months following the 2018 M_w7.5 earthquake on the Palu-Koro fault (Fig. 1B), which most likely results from deep afterslip on and below the coseismic fault surface. However, this study only incorporated one measurement on the North Arm (CTOL/TOLI in Fig. 2). Moreover, while deep afterslip explains the postseismic displacements near the Palu-Koro fault it cannot account for the amplitude of postseismic deformation at CTOL/TOLI, which lies relatively far from the coseismic rupture (Nijholt et al., 2021). A plausible explanation for this mismatch is that additional surface motions result from triggered aseismic slip on the Minahassa subduction interface, rather than on the Palu-Koro fault. In the first section of our current study, we expand upon the GNSS time series used in Nijholt et al. (2021) and investigate the entire >20-year database of GNSS data from North Sulawesi. We determine interseismic velocities and find several occurrences of surface positions that are not in line with the interseismic velocities, i.e. transient surface motion (Fig. 2). In particular, newly collected data points on the North Arm after 412 days since the 2018 Palu earthquake show cumulative offsets (Δ_{412}) that display a coherent

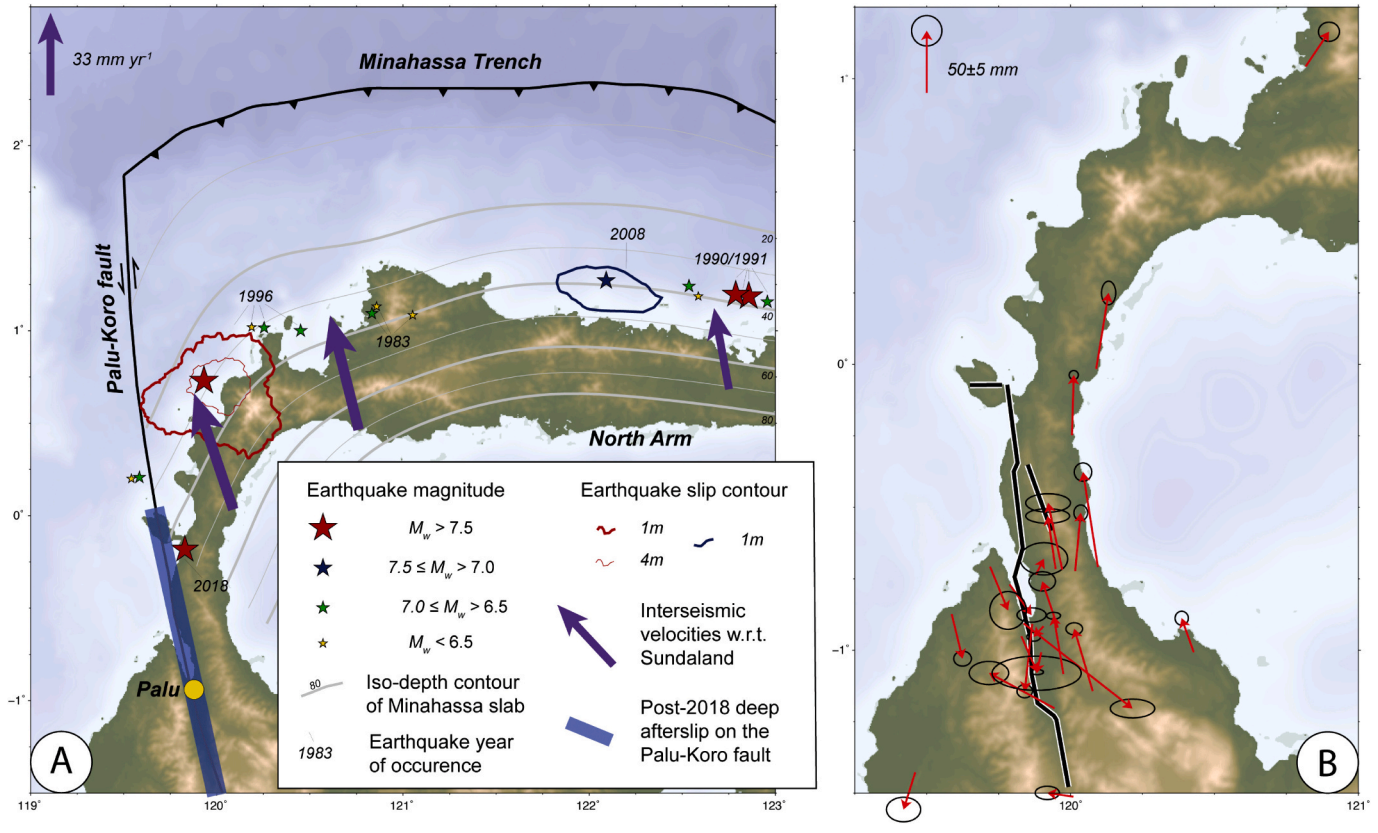

Fig. 1. A. Study region. Thick black lines outline two major fault interfaces in North Sulawesi. Gray lines are iso-depth contour lines of the Minahassa subduction interface. Coloured stars represent $M_w > 6$ earthquake locations, with coloured lines showing the ~ 50% maximum slip contour of the two largest earthquakes in the past 25 years (based on the "Finite-Fault Archives" of the USGS and "The Source Models of Large Earthquakes" of the California Institute of Technology Tectonics Observatory, both accessed online 22nd May 2023). Blue line depicts the afterslip on the Palu-Koro fault following the 2018 rupture (Nijholt et al., 2021). Purple arrows indicate some representative, interseismic GPS velocities with respect to Sundaland (see e.g., Socquet et al., 2006). B Surface fault trace (black lines) of the shallow segments that ruptured during the 2018 Palu earthquake (Simons et al., 2022) and post-seismic surface displacements after 325 days (Nijholt et al., 2021). (For interpretation of the references to colour in this figure legend, the reader is referred to the web version of this article.)

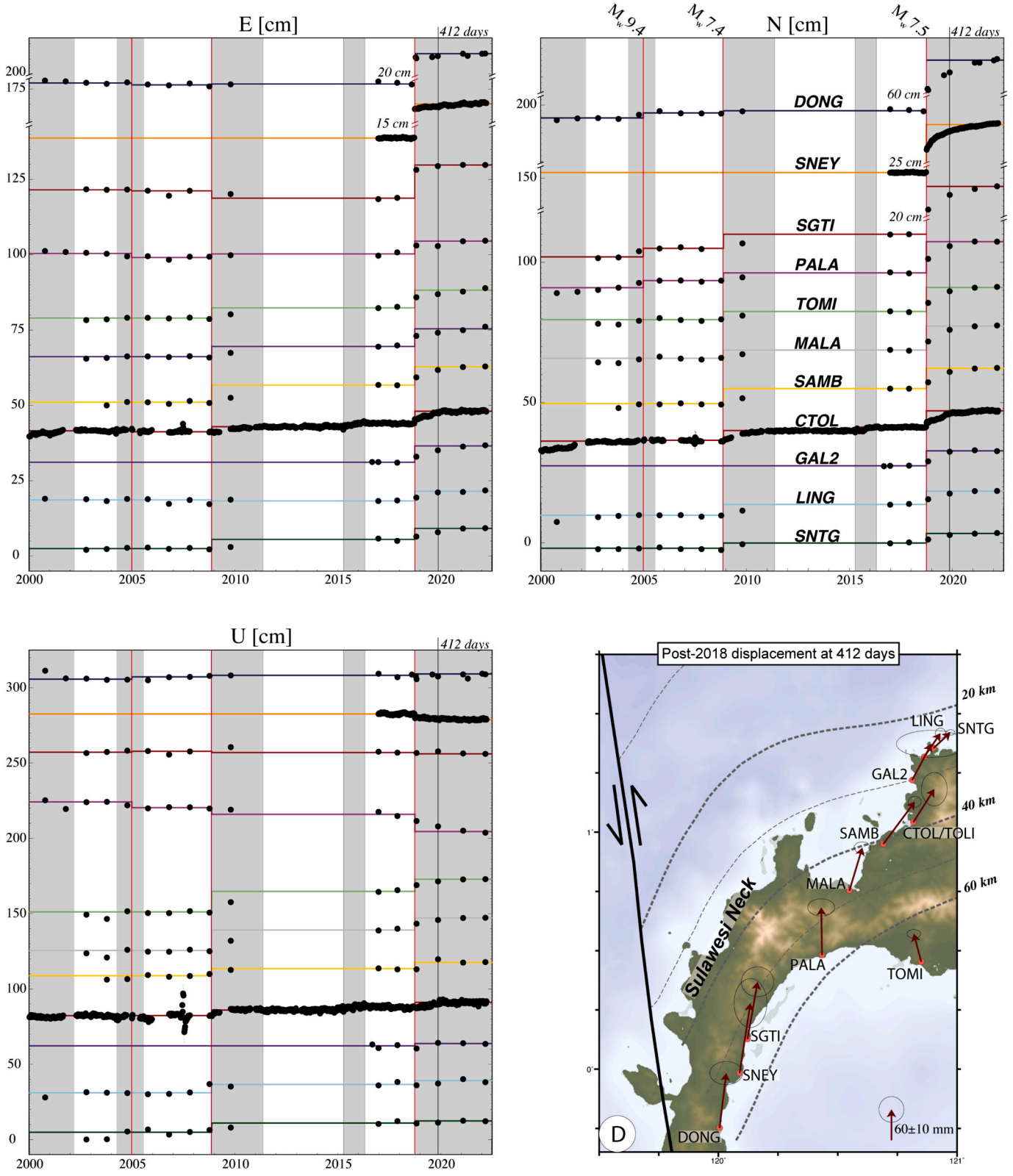

Fig. 2. Detrended continuous and campaign GNSS time series of the East (A), North (B) and Up (C) components ordered from south (top) to north (bottom). Gray domains indicate episodes of transient deformation. Red lines indicate major earthquakes: the M_w 9.22004 Sumatra-Andaman earthquake, the M_w 7.42008 Minahassa earthquake and M_w 7.52018 Palu earthquake. D Location of GNSS monuments and cumulative post-seismic offsets Δ_{412} (i.e., 412-day post-seismic positions corrected for interseismic trend and coseismic offsets) with confidence intervals displayed at the 95% level. (For interpretation of the references to colour in this figure legend, the reader is referred to the web version of this article.)

pattern with increased surface motions towards the Minahassa trench (Fig. 2D). In the subsequent sections of our study, we take a Bayesian approach to determine the likelihood that a combination of afterslip on the Palu-Koro fault and short-term, transient slow slip at the Minahassa plate interface following the 2018 Palu earthquake explains these surface motions after 412 days in a single inversion.

2. GNSS observations

2.1. GNSS data processing

We process the dual frequency GNSS dataset with a 30 s sampling rate from continuous and campaign GPS observations from 2000 to 2021. We use the zero-differencing, scientific GIPSY-OASIS II software version 6.4 (Jet Propulsion Laboratory, 2017) in the global reference frame solution of IGS, named IGS14 (Rebischung and Schmid, 2016). The IGS14 solution is based on the International Terrestrial Reference Frame 2014 (ITRF2014) (Altamimi et al., 2016). We adapted the GIPSY-OASIS software to also process data from the new block III GPS satellites, which have become operational since 2019 (GPS 74–78). We obtain precise ephemeris of GNSS satellites with Earth rotation parameters (ERP) in a non-fiducial style in IGS14 from the Jet Propulsion Laboratory (JPL). Following Simons et al. (2019), we compute non-fiducial daily position solutions with GIPSY and without pre-constrained reference positions. Next, we use daily transformation parameters to align the daily positions with IGS14 using JPL-supplied X-files. In a final step, we weekly average station positions to screen for any outliers and thereby improve reliability of the coordinate solutions.

2.2. Time series analysis approach

We fit a parametric model through the GNSS-derived positions to interpret the changes in position as a superposition of tectonic contributions. We depict the detrended timeseries in Fig. 2. In a weighted least-squares sense we estimate a constant interseismic velocity, coseismic jumps and displacements during transient episodes. We parametrize transient displacements as cumulative offsets; given that the vast majority of our observations are campaign style, this represents a purposely simple yet effective solution to determine non-interseismic motion that greatly exceeds the noise and has a coherent signal across multiple stations (see e.g., Klein et al., 2018). The estimates are made per east, north and up component in order to properly ascertain the interseismic trend prior to 2018 and determine the cumulative displacements for each transient episode. We use:

$$P(t) = P_0 + v \bullet t + \sum_{i=1}^{N} \Delta P_i^E H^E\left(t_i^E\right) + \sum_{j=1}^{M} \Delta P_j^T H^T\left(t_j^T\right)$$

Where the position $P(t)$ is the modeled position and thus a sum of the starting position P_0 for the given component (E, N or U), the interseismic velocity v and the offsets ΔP_i^E and ΔP_j^T for earthquakes and transient episodes, respectively. For each component of a timeseries, transient episodes are included as Heaviside step functions H. The length of a transient episode is not equal for all stations, but it is for all components of a station; for example, CTOL/TOLI has two transient episodes between 2008 and 2017 whilst the campaign stations take this entire time period as one big transient episodes as they were measured only once in this time period. N is the total number of earthquakes (2004, 2008, 2018) per station that start at times t_i^E, and M is the total number of transient episodes per station. These times t_i^E are designated manually. For the fit, we do not take into account data from transient episodes (likewise we exclude outliers). Hence, observations from transient periods do not affect the estimated interseismic trend. The time step t_j^E for a transient episode is defined in the middle of a transient episode. We use weighted least squares to fit the above equation to the data, with inverse variances as weights. We manually identify transient episodes as time-varying deviations from the trend. We add a table of the estimated parameters from the least-squares inversion in the Supporting Data at the 4TU repository (Nijholt et al., 2024) and show the time series of individual stations in Figs. S1–11. When the interseismic trend is subtracted from the positions, both the long-term campaign and continuous time series in North Sulawesi display recurrent deviations (Fig. 2); many of these can be determined most clearly in the continuous time series of CTOL/TOLI.

For the 2004, 2008 and 2015 transients we use the weighted least squares cumulative offset estimates. Because of the large magnitude of the 2018 transients, we use the detrended weekly averaged positions instead, that contain the coseismic and postseismic cumulative offsets since the 2018 earthquake and that have the following uncertainties:

$$\sigma_{t,co+post} = \sqrt{\sigma_t^2 + \sigma_v^2 (t - t^{E_{2018}})^2}$$

With σ_t the standard deviations from the weekly averaged positions, and σ_v the interseismic velocity uncertainties from the weighted least squares inversion, t time and $t^{E_{2018}}$ the time since the 2018 earthquake. From the post-2018 detrended displacements we subtract the coseismic offsets from Simons et al. (2022), which have a better coseismic estimate than the above weighted least squares estimation due to the inclusion of corrections for early postseismic motions in Simons et al. (2022).

The uncertainty of the cumulative postseismic offsets Δ_{412}, $\sigma_{412,post}$, is solely dependent on the standard deviations of the coseismic displacements σ_{co} (from Simons et al., 2022) and of the detrended positions at 412 days $\sigma_{412,co+post}$:

$$\sigma_{412,post} = \sqrt{\sigma_{412,co+post}^2 + \sigma_{co}^2}$$

Table S1 provides cumulative offsets Δ_{412} and its uncertainties for all GNSS sites.

2.3. Time series analysis results

In Fig. 2 we depict the detrended time series of the east, north, and up components for the stations in North Sulawesi, with colour-coded lines per station. The detrended time series show transient episodes as deviations from the horizontal line. We order the stations in Fig. 2 from south (top) to north (bottom) as the positions changes in the north component are largest for the southernmost station following the 2018 Palu earthquake.

CTOL/TOLI is the station name we use here as CTOL is the continuation of the older site TOLI. This station clearly displays four larger transient episodes (Fig. 2): the first spans from the start of the timeseries into 2002, the second directly follows the 2008 subduction earthquake, the third crosses 2015–2016, and the fourth starts directly after the 2018 Palu earthquake. The transient motion in the first two years of recording shows a complex signal possibly induced by the 1996 earthquake. Walpersdorf et al. (1998) and Vigny et al. (2002) report similar transient motion with a dominant North component following the 1996 earthquake for station in the Palu Bay area, east of the Palu-Koro fault. We also observe a transient in 2004 with the largest offsets in the north component at the (southern) stations, closest to the Palu-Koro fault. The 2008 and 2015 transients, as recorded by CTOL/TOLI, can only be seen as a cumulative offset for campaign stations as they had not been measured regularly over this time span. In Fig. 3, we display cumulative displacements of these three transient episodes to show they are of similar order of magnitude, spatially coherent and their magnitude exceeds the observational uncertainty. All displacements are northward during transient episodes; through every transient episode there is a position change that qualitatively agrees with both the direction of strike-slip motion of the Palu-Koro fault as well as with slip on the Minahassa subduction interface. Transient displacements in the east direction are much smaller in magnitude, and are not consistently

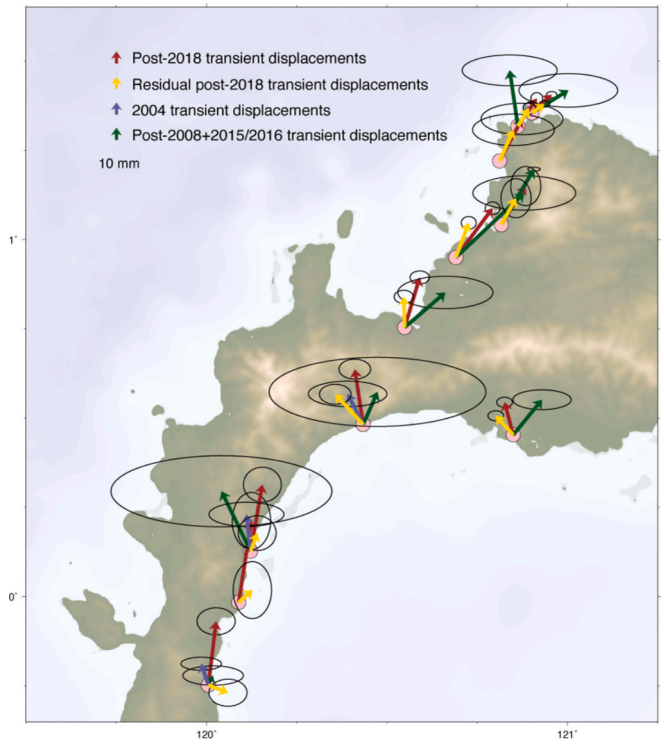

Fig. 3. Comparison of transient displacements at the surface with their 95% confidence limits. Red-brown arrows show Δ_{412}. Blue arrows show the cumulative displacements determined at the three stations for the transient that started in 2004 (σ_{2004} follows from the weighted least squares inversion); it was not included as a transient offset for the other stations in the parameterization. Green arrows show the cumulative displacements determined for the stations in NW Sulawesi ($\sigma_{2008+2015}$ follows from the weighted least squares inversion). For CTOL/TOLI, we add the cumulative displacements for these two periods and compute the new standard deviation $\sigma_{2008+2015} = \sqrt{{\sigma_{2008}}^2 + {\sigma_{2015/2016}}^2}$. (For interpretation of the references to colour in this figure legend, the reader is referred to the web version of this article.)

positive or negative. The post-2018 time series of CTOL/TOLI (Fig. S11) does not have a temporal shape typical for afterslip, i.e., a logarithmic decay function. Rather, it appears as a superposition of a decaying trend and a slowly increasing and then decreasing signal with the peak velocity at about 340 days. As the Minahassa subduction interface is located at depth below the GPS station, this second trend is possibly the imprint of a deep SSE. A slow rise after the 2018 earthquake is followed by a rapid acceleration with a subsequent gradual deceleration in transient motion, a typical temporal characteristic of SSEs (Kostoglodov et al., 2003; Ozawa et al., 2002; Outerbridge et al., 2010; Wallace and Beavan, 2010).

Following the 2018 Palu earthquake, the largest magnitude post-seismic transients have been observed near Palu (Nijholt et al., 2021). These seem to continue at least until the end of the recorded positions (Fig. 2). The stations on the North Arm report slightly decreasing magnitudes from south to north and sway from a slight west-component at PALA and TOMI, to a larger east-component from SAMB northwards (Figs. S1-S11). The six northernmost stations all show uplift post-2018, which decreases northwards. Other stations on the North Arm show no significant vertical motion. The pattern of horizontal cumulative offsets up to 412 days after the 2018 Palu earthquake (Fig. 2D) from the continuous and campaign stations is spatially coherent and significantly surpasses the noise level for all three components. This thus hints at a tectonic signal that we interpret in the following sections.

2.4. Integrating heterogeneous campaign data following the 2018 earthquake

We consider that the Δ_{412} observations potentially result from both 1) Palu-Koro fault afterslip, and 2) slow slip on the Minahassa subduction interface. Namely, we expect the stations on the North Arm to be affected by both slip on the subduction interface as well as Palu-Koro afterslip (Nijholt et al., 2021), while the sites near Palu will be too distant to the Minahassa subduction zone to be affected significantly by slow slip. This view is also justified by the timeseries in the Palu area (Fig. 4), which do not show any indication of the accelerating and decelerating motions that we observe for CTOL/TOLI in Fig. 2. These time series follow a single decaying curve, indicating that the surface motions near Palu solely result from post-seismic motion directly following the 2018 earthquake. This is most likely due to afterslip on the Palu-Koro fault (Nijholt et al., 2021).

As the right panel of Fig. 4 shows, the time for which we have observations available is not uniform; at the North Arm we have data at 412 days since the earthquake (Δ_{412}), whereas for the Palu area we have data at 325 days after the 2018 event (Δ_{325}). The Palu-Koro afterslip thus has to be estimated at 325 and 412 days. To bridge the temporal gap between the observations at specific times, we consider the time series of detrended displacement for three continuous stations (WATP, SNEY and TOBP; Fig. 4). As these sites show very consistent temporal behavior, we assume that the Palu-Koro afterslip at 325 and 412 days differs only by a scale factor, and that the time series of the three continuous sites can be used to estimate this scale factor.

In Fig. 4, we show the detrended time series following the 2018 Palu earthquake, and fit an exponential decay function with the same decay constant τ but station-based amplitudes and starting (coseismic) offsets through these time series:

$$P(t) = \Delta P^E + A_P\left(1 - e^{-t/\tau}\right)$$

where ΔP^E is the coseismic position change from the 2018 earthquake, t is the time since the earthquake and A_P is the total amount of postseismic motion as t goes to infinity. The decay time constant τ controls how quickly the modeled $P(t)$ approaches $\Delta P^E + A_P$. The choice for an exponential decay function is somewhat arbitrary: the time series could also be fit well with a logarithmic function. Both would fit this kind of post-seismic data conveniently (e.g., Johanson and Bürgmann, 2010), but the exponential decay function has the advantage that the function approaches $\Delta P^E + A_P$ as t increases, instead of infinity in the case of logarithmic functions.

We take a Bayesian approach to fit the exponential decay function, using the same methodology as for estimating the Palu-Koro afterslip and the Minahassa slow slip, outlined in the subsequent section. We do not add additional terms to improve the fit in the first few weeks following the 2018 Palu earthquake. Hence, we treat the coseismic position change as a variable in our Bayesian search to fit the decaying time series. In the remainder of the study, we use the coseismic jumps from Simons et al. (2022) to determine Δ_{412}. We find the decay constant to be about 200 days and have added the results of the fitting exercise underlying Fig. 4 in Nijholt et al. (2024). The fit provides the scale factor σ per station and per component for the Palu-Koro afterslip between 325 and 412 days:

$$\sigma = \frac{\left(1 - e^{-412/\tau}\right)}{\left(1 - e^{-325/\tau}\right)}$$

The extrapolation of the afterslip contribution to 412 days only adds a few % to the cumulative post-seismic surface motions.

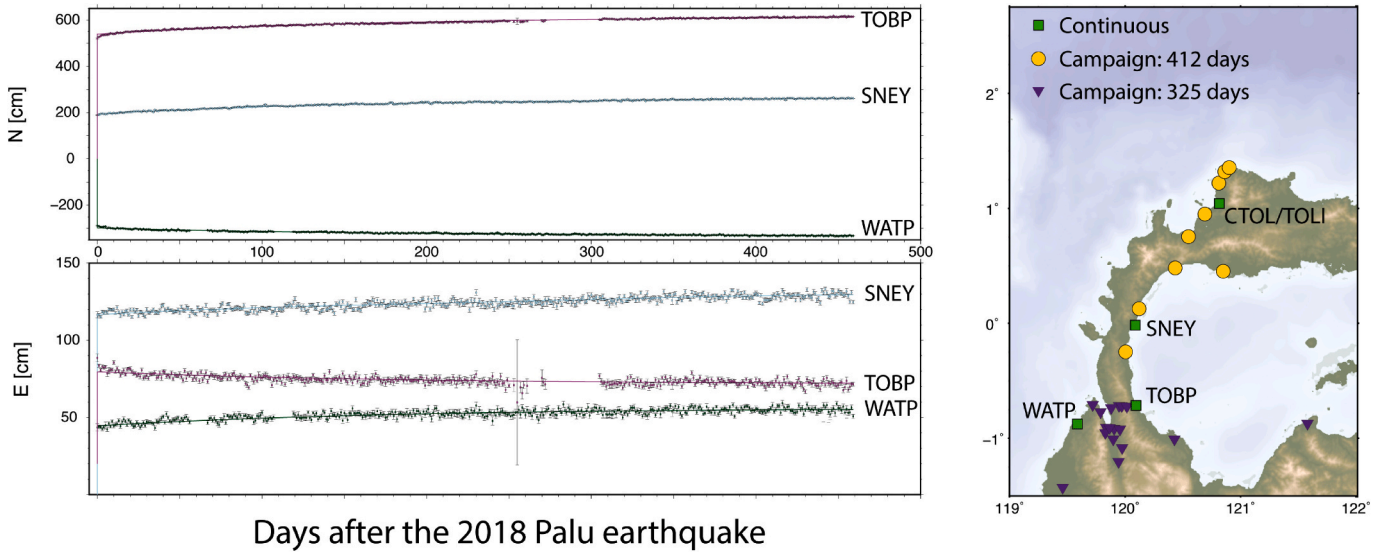

Fig. 4. Detrended continuous time series for three stations in northwest Sulawesi, fit by exponential decay functions with a single decay constant of about 200 days. The map in the right panel shows their locations. This map also includes locations of the campaign stations for which data was recorded at 412 days (yellow circle) and 325 days (purple triangle; Nijholt et al., 2021). (For interpretation of the references to colour in this figure legend, the reader is referred to the web version of this article.)

3. Fitting the GNSS data with finite fault slip models

3.1. Bayesian search methodology

We use a simple Metropolis-Hastings algorithm to estimate Minahassa slow slip and Palu-Koro afterslip; we stepwise (randomly) search the parameter space of a model to best constrain the posterior probability distribution of relevant model input parameters (m) (Tarantola, 2005; Herman and Govers, 2020). In this we consider that the posterior probability distribution of the parameters $P(m_{inp}|d_{obs})$ is proportional to the product of the likelihood of observing the data (d) given the model (G) $P(d_{obs}|m_{inp})$ and the prior information $P(m_{inp})$:

$$P(m_{inp}|d_{obs}) \propto P(d_{obs}|m_{inp})\ P(m_{inp})$$

$$\propto \frac{1}{(2\pi)^{\frac{N}{2}}|C_B|^{\frac{1}{2}}} exp\left\{\frac{-1}{2}(\overline{d_{obs}} - G\overline{m_{inp}})^T C_B{}^{-1}(\overline{d_{obs}} - G\overline{m_{inp}})\right\}$$

where C_B is an error-covariance matrix and N is the number of observations. We assume for the prior information that it conforms to a uniform distribution bounded by assigned parameter ranges. We consider C_B a diagonal matrix that consists of data errors (e.g., uncertainty of the residual postseismic displacements) and a model prediction error of 0.1 (which are normalised by the magnitude of observed GNSS offsets (Minson et al., 2013)). To match the data after 325 days we only take afterslip on the Palu-Koro fault into account. For the North Arm data at 412 days the inversion accounts for both the Palu-Koro afterslip (extrapolated from the slip distribution at 325 days using the scale factor $\mathcal{O}$) as well as slow slip on the Minahassa subduction interface.

3.2. Finite fault representation of slip distribution

Okada (1992) formulations of a series of buried dislocations in an elastic half-space form the basis of our Palu-Koro afterslip model, using a shear modulus of $32 \bullet 10^9$ Pa and Poisson ratio of 0.25. We build on the Nijholt et al. (2021) geometry of 37 × 15 km patches by adding a maximum of two additional segments to the south and six additional segments towards the north: it is possible that afterslip extended beyond the coseismic slip segment, affecting surface motion at the North Arm. Following Nijholt et al. (2021), for each Palu-Koro slip patch, the slip magnitude can vary in the range 0–5 m and the rake can differ up to ±45° with respect to pure left-lateral slip.

We model cumulative slow slip on the Minahassa subduction interface through a series of triangular dislocations (Fig. 5) buried in an elastic half-space (Meade, 2007). The topology of fault patches is a modification of the Slab2 geometry (Hayes et al., 2018) where the lateral termination of the subduction interface abuts the Palu-Koro fault, based on the seafloor bathymetry of Hall (2018) and the 2018 co-seismic slip distribution (Fig. 1). We take the maximum depth of the bottom segment of the finite fault model at 70 km. The slip magnitude of each potential slip patch is variable and ranges between 0 and 0.6 m. We let the rake of each patch vary within 15° from the local plate convergence direction (Greenfield et al., 2021) at that longitude. We calculate the resolving power of the GNSS network by determining the sum of modeled GNSS station displacements due to unit dip- and strike-slip motion per patch, divided by the patch area (Loveless and Meade, 2011). We find that slip cannot be resolved equally well for all patches; we test three different combinations of fault patch geometries based on the resolving power that limit the choice of patches that we include in the models. In our main model, we only consider patches that exceed a power of $1 \bullet 10^{-10}$ m^{-1}, as shown in Fig. 5 by the yellow contour.

4. Bayesian inversion results

The Bayesian mean model solution matches the cumulative surface displacements after 325 days (Fig. 6A and B) and 412 days (Fig. 7A and B). The mean posterior afterslip distribution on the Palu-Koro fault (Fig. 6C) is similar to the distribution determined by Nijholt et al. (2021) wit h the largest contribution of slip from the deeper segments. The contribution from Palu-Koro afterslip mostly underpredicts the CTOL/TOLI observation, and to a lesser degree the sites on the Sulawesi Neck. However, when combining the extrapolated afterslip contribution with the slow slip distribution for the subduction interface the North Arm displacements are well explained (Fig. 7A). The mean posterior slow slip distribution on the Minahassa interface (Fig. 7C) shows the largest slip magnitudes on a patch at 30–50 km depth, localizing below and just west of Dondo Bay. The mean slip reaches a magnitude of 40 cm, which exceeds the posterior uncertainties (Fig. 7D). The group of patches with the best constrained slip (the orange domain of Fig. 7D) releases a total

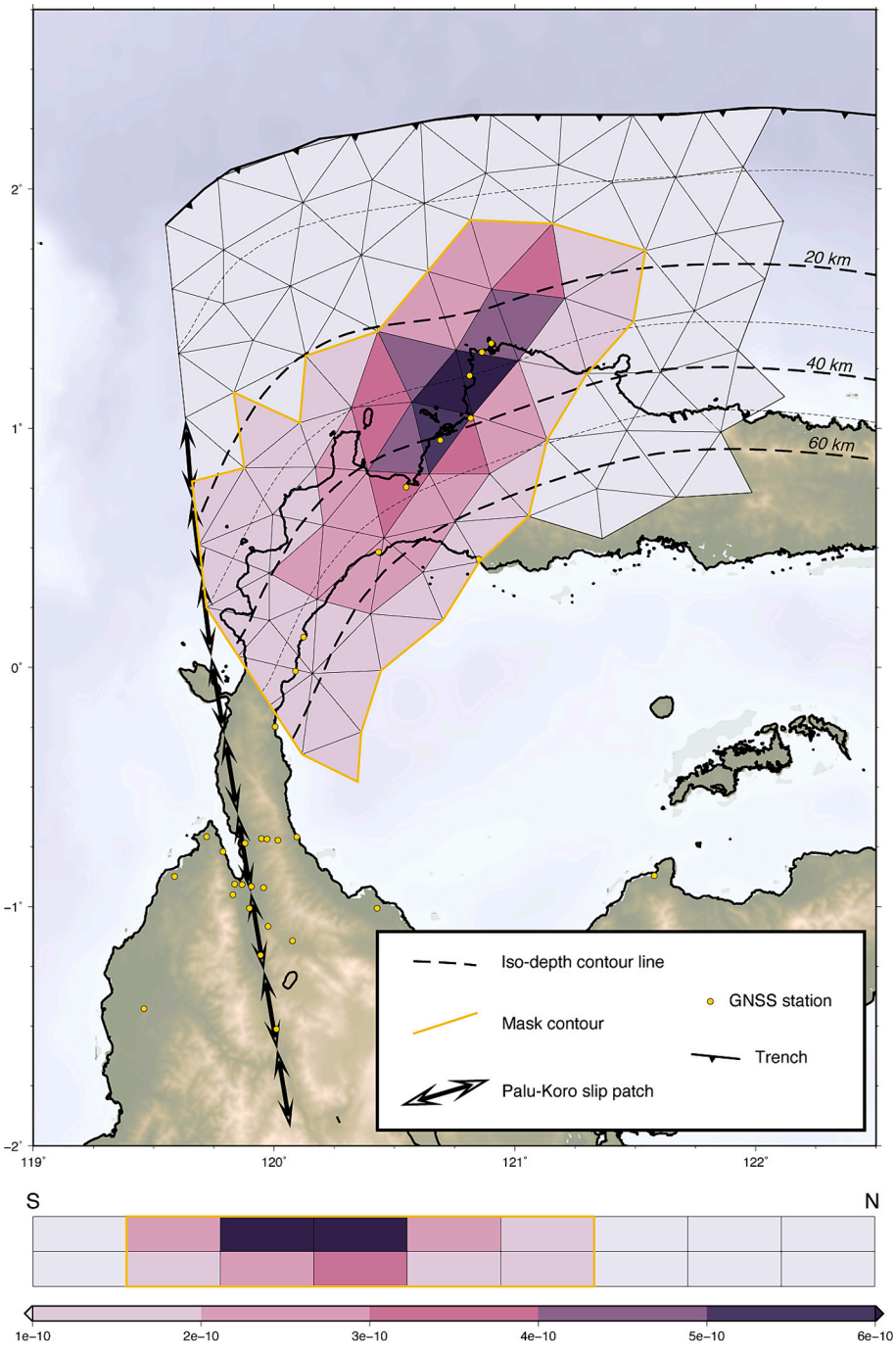

Fig. 5. Overview of the resolving power of the GNSS station distribution in NW Sulawesi for both our fault interfaces: the sum of GNSS station displacements due to unit dip- and strike-slip motion per patch, divided by the patch area. The yellow contour denotes the 'large' mask used in the main text inversion. This large mask only contains patches that have a resolving power higher than $1 \bullet 10^{-10} \mathrm{m}^{-1}$. (For interpretation of the references to colour in this figure legend, the reader is referred to the web version of this article.)

moment magnitude of 6.7, whilst the mean of the posterior total moment magnitude release on the interface equals 7.2 (with the largest fraction not exceeding the uncertainty individually, Fig. 7E). Slip also occurs outside of those well-resolved patches, but the exact location is less certain. There is no strong trade-off between resolved slip on the two interfaces (Fig. 7E): both sources of slip are needed to explain the surface displacements at 412 days.

The slip patch near Dondo Bay remains a stable feature under various assumptions of the Bayesian approach: alternative choices in the slip magnitude range (Figs. S13–14), or the use of a less or a more restrictive power mask (Figs. S12 &15) also result in significant slip on this segment of the subduction interface. Additionally, an alternative choice in the model error gives a similar slip distribution for the Minahassa subduction interface (Figs. S16–17).

5. Discussion: signs of multiple episodes of transient deformation

GNSS measurements at the continuous station in the north of Sulawesi (CTOL/TOLI, Fig. 2) indicate that an episode of transient deformation started soon after the 2018 Palu earthquake. Combining data from this continuous station with other campaign stations reveals a

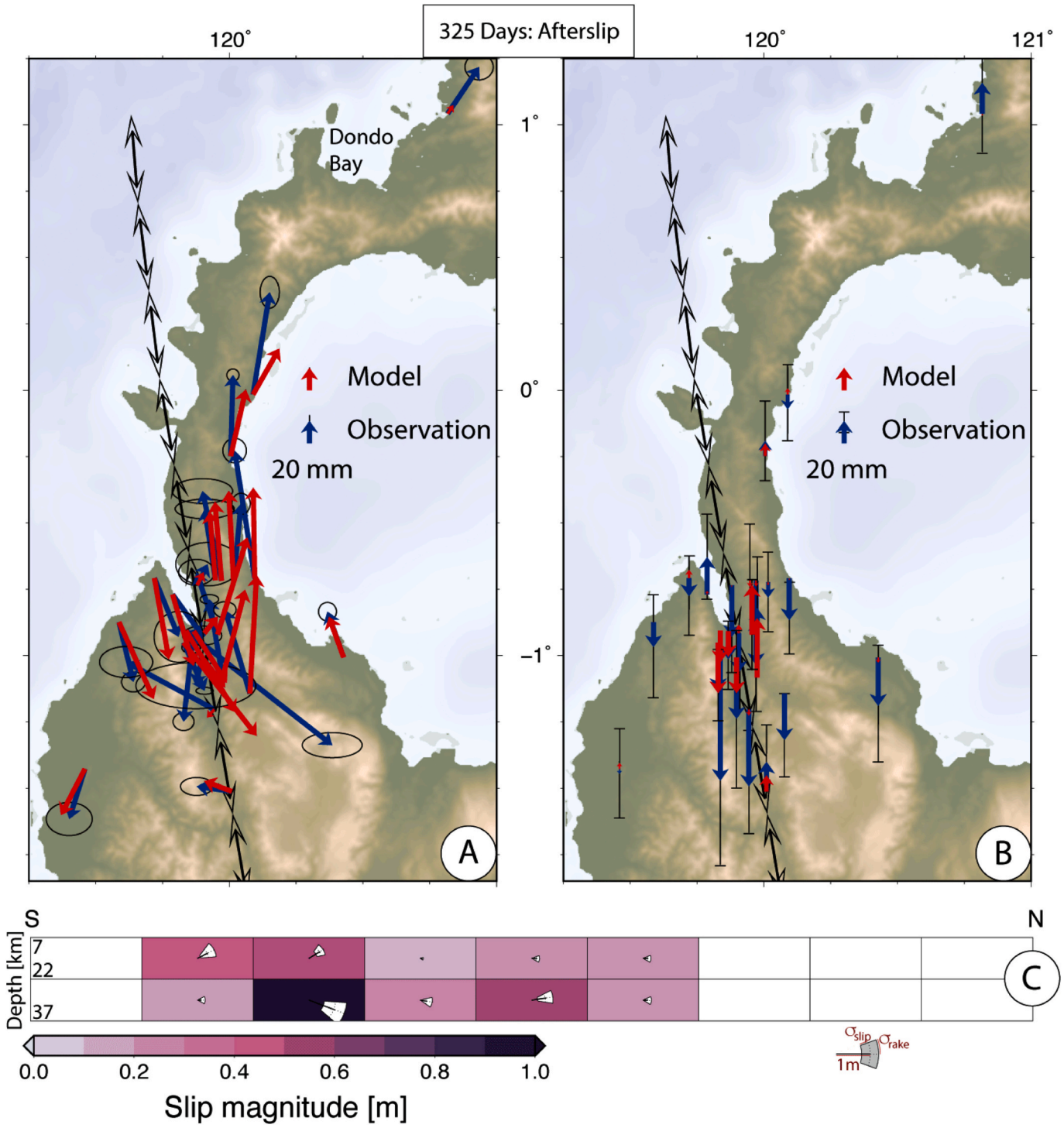

Fig. 6. Panels A and B depict the horizontal and vertical vectors of the cumulative 325 days residual offsets (red) due to Palu-Koro afterslip (blue). C The finite fault representation of the inferred mean, deep afterslip on the Palu-Koro fault plane. Swaths indicate their 2-sigma bounds. Patches in white depict zero slip in the forward model. (For interpretation of the references to colour in this figure legend, the reader is referred to the web version of this article.)

coherent transient deformation signal. Our Bayesian methodology provides a consistent inference of a combination of two, separate physical mechanisms causing surface motion: deep afterslip on the Palu-Koro fault, which mainly affects the Palu region (Nijholt et al., 2021) (Fig. 6C), and a (possibly triggered) aseismic SSE on the Minahassa subduction interface, which mainly affects displacements on the North Arm (Fig. 7C). We cannot constrain the spatio-temporal evolution of the post-2018 SSE, due to sparse temporal resolution of the data. After 412 days, surface velocities at the North Arm have largely returned to their interseismic value, whilst in the Sulawesi Neck and Palu region most stations show ongoing transient displacements (Fig. 2). The 2018 Palu earthquake incited a small Coulomb stress change on the subduction interface (Fig. S18). As the SSE is located just at the edge of a small positive stress change, this indicates an apparent near-critical state of this segment prior to the SSE in case this Coulomb stress change triggered the SSE; several studies indicate that SSEs can be triggered by small stress changes (e.g., Rubinstein et al., 2008; Han et al., 2014; Wallace et al., 2017). Dynamic stress changes from the 2018 rupture

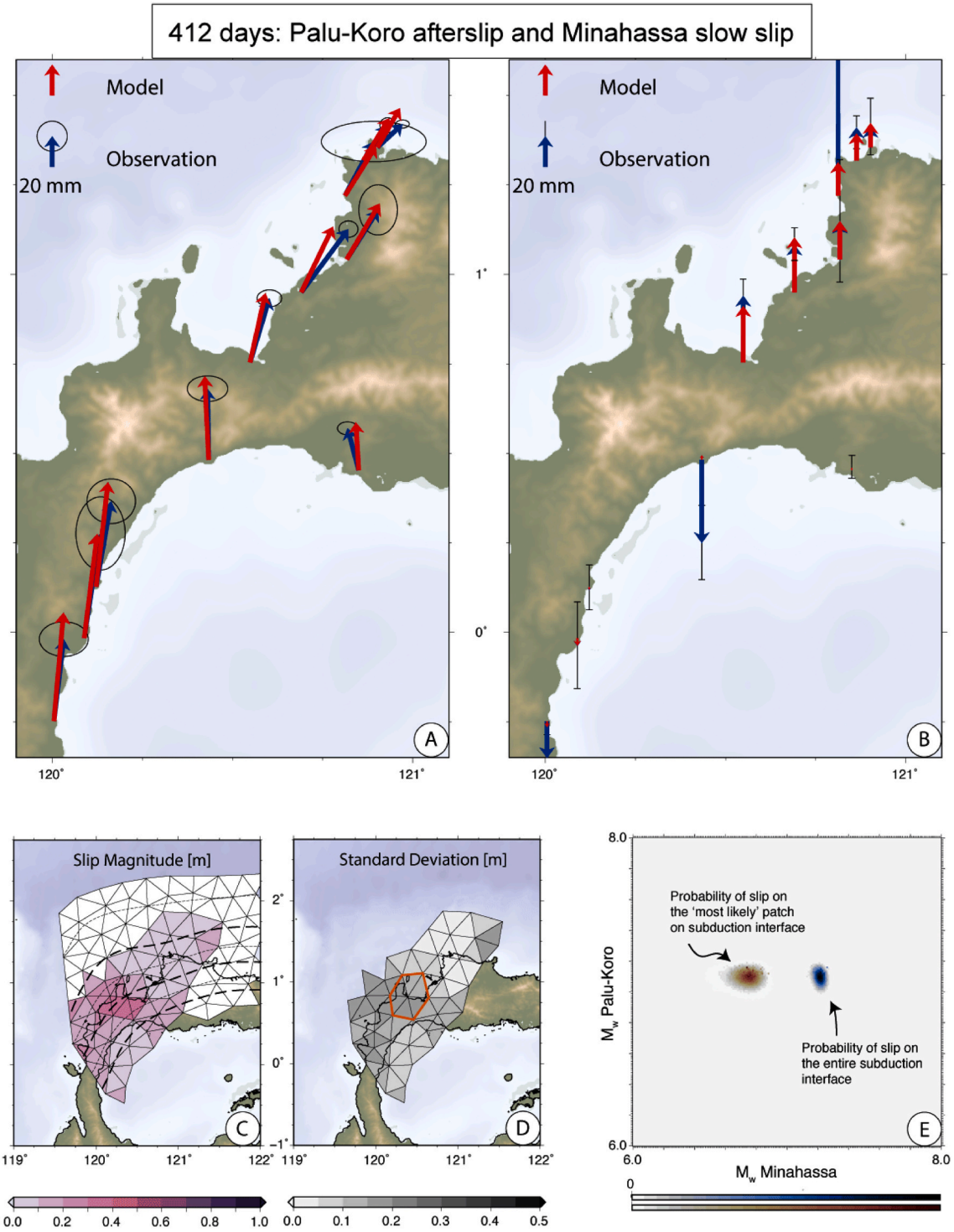

Fig. 7. Panels A and B depict the 412-day residual offsets (red) and model predictions (blue) based on a combination of the extrapolated Palu-Koro afterslip and the mean posterior slip on the Minahassa subduction interface for the horizontal and vertical components, respectively. Uncertainties at the 95% level. C Mean posterior slow slip distribution. D Standard deviations for the posterior slow slip distribution. Orange outline shows the SSE patch that significantly exceeds the uncertainties. E 2-D marginal probability for the moment magnitude released on the subduction interface and the Palu-Koro fault. (For interpretation of the references to colour in this figure legend, the reader is referred to the web version of this article.)

could also trigger the SSE if these stresses were large enough, as has been shown in other regions (Miyazawa and Mori, 2005, 2006; Wei et al., 2018, Cruz-Atienza et al., 2021). However, the strongest direction of energy dispersion was in a southward direction for this supershear rupture (Bao et al., 2019). Building on the data and model of Nijholt et al. (2021), with new observations and a Bayesian inference of slip on two faults in a single optimization, we can now qualitatively state that two, distinct fault interfaces have experienced a slip episode in the wake of the 2018 Palu earthquake with significant moment released. We find no trade-off in slip on either interface in the estimation.

This subduction interface has only experienced a few $M_w > 6$ earthquakes over the past three decades (Figs. 1 & 8). Our estimate

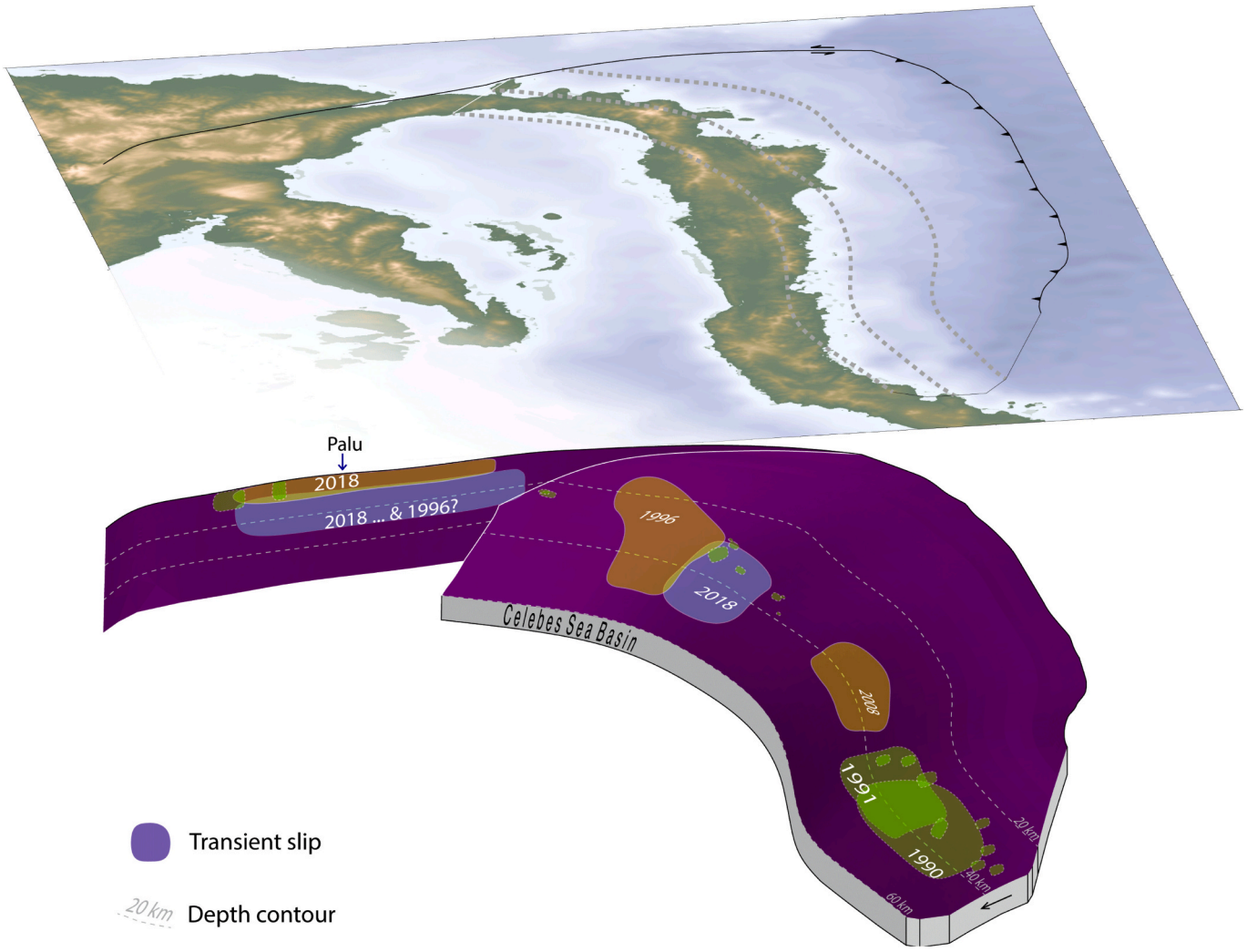

Fig. 8. Synoptic view of the plate tectonic setting in North Sulawesi, including the locations of the $M_w > 6$ earthquakes. The post-2018 SSE is located next to the 1996 rupture patch, in an area where hardly any large magnitude earthquakes have occurred over the past few decades.

locates the post-2018 SSE directly east of the 1996 asperity. Seismic activity did not increase on the subduction interface following the 2018 earthquake, similar to previous episodes of transient deformation, according to the data presented in Supendi et al. (2020) and Nijholt et al. (2021). Previous episodes of transient surface motion had smaller magnitude cumulative offsets (Fig. 2). Only CTOL/TOLI has recorded the imprints of these transients, because the temporal coverage of the GNSS network during the 2000, 2008 and 2016 transients is poor. A similar fault interaction has been suggested by Walpersdorf et al. (1998) who showed that the Palu-Koro fault slip rate greatly exceeded its interseismic magnitude by a factor of >2 in the years following the 1996 subduction interface rupture. Transient motion on the (northern section of the) Palu-Koro fault has the potential to influence seismic hazard in North Sulawesi, pushing other faults closer to or further from failure. With the current data coverage, we can confirm episodic transient deformation in North Sulawesi on a 4–5 years interval. We only have sufficient data to ascribe the post-2018 transient specifically to slow slip on the subduction interface of the Minahassa trench.

The tectonic setting of North Sulawesi conforms to a Subduction-Transform Edge Propagator setting: a subduction interface that transitions into a strike-slip fault zone at its termination (Govers and Wortel, 2005). Other tectonic settings for which SSEs occur close to the lateral end of a slab are the Hellenic subduction zone (Mouslopoulou et al., 2020), and the Hikurangi subduction zone (e.g., Wallace, 2020). Several SSEs on the Hikurangi interface (New Zealand) occurred near the western termination of the slab (Wallace and Beavan, 2010). On the Hikurangi interface, deep and shallow SSEs both occur as the depth of strong coupling changes along-strike the Hikurangi interface (Wallace and Beavan, 2010). Strong lateral changes in coupling also influences crustal fault activity (Hamling and Wallace, 2015). Potentially this is also the case for the Minahassa interface.

The presence of the post-Palu 2018 SSE within (and below) the seismogenic zone of the Minahassa subduction interface (Fig. 8) influences the locking state of this plate boundary (along-strike). Especially considering the notion that 20–70% of the slip deficit can be accommodated through SSEs (e.g., Wallace and Beavan, 2010; Takagi et al., 2019). The mechanisms of stress transfer between subduction interfaces and STEP faults are a second unknown factor. The current assessments of seismic hazard are therefore limited. Future advances to better understand the seismic hazard of North Sulawesi can be made by improving availability of high-resolution observational evidence to discern a locking pattern or tremor activity on both the Palu-Koro fault and the Minahassa subduction interface, as these two faults are expected to interact continually. Activity on the subduction megathrust and the juxtaposed Palu-Koro fault may result in a devastating interplay, through a single mega-event that incorporates slip on both faults or from triggered ruptures due to slow slip activity.

6. Conclusions

GNSS observations in North Sulawesi highlight transient surface motions in the wake of the 2018 Palu earthquake. Through a Bayesian inversion of slip on two interfaces, we infer that slow slip on the Minahassa subduction interface in combination with deep afterslip on the Palu-Koro fault is the most likely explanation for the observed surface motions. We thus note the first recording of a slow slip event on this subduction interface. The seemingly-triggered SSE is located just east of the 1996 M_w7.9 rupture, and has a magnitude of at least M_w6.7. Further evaluation of 20 years of continuous and campaign data reveals multiple, older episodes of transient motion with an interval of 4–5 years. A continual interplay between the Minahassa subduction interface and the Palu-Koro strike-slip fault likely exists based on our geodetic observations, affecting the seismogenic potential of both parts of this tectonic system.

CRediT authorship contribution statement

N. Nijholt: Writing – review & editing, Writing – original draft, Visualization, Validation, Software, Methodology, Investigation, Funding acquisition, Formal analysis, Conceptualization. **W. Simons:** Writing – review & editing, Writing – original draft, Visualization, Validation, Supervision, Software, Resources, Project administration, Methodology, Funding acquisition, Formal analysis, Data curation, Conceptualization. **R. Riva:** Writing – review & editing, Validation, Supervision, Methodology. **J. Efendi:** Formal analysis, Data curation. **D. Sarsito:** Formal analysis, Data curation. **T. Broerse:** Writing – review & editing, Validation, Methodology.

Declaration of competing interest

The authors declare that they have no known competing financial interests or personal relationships that could have appeared to influence the work reported in this paper.

Data availability

GNSS data (RINEX files, and a file of position offsets w.r.t. the interseismic trend) and model output files are archived at the institutional repository of TU Delft.

Acknowledgements

The continued (long-term) operation of the GPS stations in Central Sulawesi, Indonesia data has been cofacilitated by the EU-ASEAN SEAMERGES (2004–2006) and GEO2TECDI-1/2 projects (2009–2013). The GPS data acquisition and research were also partly funded by grants from the Dutch NWO User Support Programme Space Research (2007–2019). We would like to express our special thanks to the local staff of the Indonesian Meteorology, Climatology, and Geophysical Agency (BMKG) offices in Palu for providing their local micro-seismic data catalog. N. Nijholt (ALWGO.2019.045) and T. Broerse (ALWGO.2018.038) are funded by the NWO.

Software for computing fault slip and surface displacements and performing the search is available online (https://doi.org/10.5281/zenodo.3894137) and we follow the methodology outlined in Herman and Govers (2020). The GPS data from the (continuous) CORS stations and campaign stations in Indonesia are available (at no cost) from BIG through http://bit.ly/corsBIG. We would like to thank the editor, Gregory Houseman, and two anonymous reviewers for their constructive comments.

Appendix A. Supplementary data

Supplementary data to this article can be found online at https://doi.org/10.1016/j.tecto.2024.230416.

References

Altamimi, Z., Rebischung, P., Métivier, L., Collilieux, X., 2016. ITRF2014: a new release of the International Terrestrial Refer- ence Frame modeling non-linear station motions. J. Geophys. Res. Solid Earth 121 (8), 6109–6131. https://doi.org/10.1002/2016JB013098.

Bao, H., Ampuero, J.P., Meng, L., et al., 2019. Early and persistent supershear rupture of the 2018 magnitude 7.5 Palu earthquake. Nat. Geosci. 12, 200–205. https://doi.org/10.1038/s41561-018-0297-z.

Bartlow, N.M., 2020. A long-term view of Episodic Tremor and Slip in Cascadia. Geophys. Res. Lett. 47 https://doi.org/10.1029/2019GL085303 e2019GL085303.

Beroza, G.C., Ide, S., 2011. Slow earthquakes and nonvolcanic tremor. Annu. Rev. Earth Planet. Sci. 39 (1), 271–296. https://doi.org/10.1146/annurev-earth-040809-152531.

Cruz-Atienza, V.M., et al., 2021. Short-term interaction between silent and devastating earthquakes in Mexico. Nat. Commun. 12 (1), 2171. https://doi.org/10.1038/s41467-021-22326-6.

Dragert, H., Wang, K., James, T.S., 2001. A silent slip event on the deeper Cascadia subduction interface. Science 292 (5521), 1525–1528.

Govers, R., Wortel, M.J.R., 2005. Lithosphere tearing at STEP faults: Response to edges of subduction zones. Earth Planet. Sci. Lett. 236 (1–2), 505–523.

Greenfield, T., Copley, A.C., Caplan, C., Supendi, P., Widiyantoro, S., Rawlinson, N., 2021. Crustal deformation and fault strength of the Sulawesi subduction zone. Tectonics 40. https://doi.org/10.1029/2020TC006573 e2020TC006573.

Hall, R., 2018. The subduction initiation stage of the Wilson cycle. Geol. Soc. Lond. Spec. Publ. 470, 415–437. https://doi.org/10.1144/SP470.3.

Hamling, I.J., Wallace, L.M., 2015. Silent triggering: aseismic crustal faulting induced by a subduction slow slip event. Earth Planet. Sci. Lett. 421, 13–19.

Han, J., Vidale, J.E., Houston, H., Chao, K., Obara, K., 2014. Triggering of tre- mor and inferred slow slip by small earthquakes at the Nankai subduction zone in Southwest Japan. Geophys. Res. Lett. 41, 8053–8060. https://doi.org/10.1002/2014GL061898.

Hayes, G.P., Moore, G.L., Portner, D.E., Hearne, M., Flamme, H., Furtney, M., Smoczyk, G.M., 2018. Slab2, a comprehensive subduction zone geometry model. Science 362 (6410), 58–61. https://doi.org/10.1126/science.aat4723.

Herman, M.W., Govers, R., 2020. Locating fully locked asperities along the South America subduction megathrust: a new physical inter-seismic inversion approach in a Bayesian framework. Geochem. Geophys. Geosyst. 21 https://doi.org/10.1029/2020GC009063 e2020GC009063.

Hirose, H., Hirahara, K., Kimata, F., Fujii, N., Miyazaki, S., 1999. A slow thrust slip event following the two 1996 Hyuganada earthquakes beneath the Bungo Channel, Southwest Japan. Geophys. Res. Lett. 26, 3237–3240.

Ide, S., Beroza, G.C., Shelly, D.R., Uchide, T., 2007a. A scaling law for slow earthquakes. Nature 447 (7140), 76–79. https://doi.org/10.1038/nature05780.

Ide, S., Shelly, D.R., Beroza, G.C., 2007b. Mechanism of deep low frequency earthquakes: further evidence that deep non-volcanic tremor is generated by shear slip on the plate interface. Geophys. Res. Lett. 34, L03308 https://doi.org/10.1029/2006GL028890.

Ishihara, Y., 2003. Major existence of very low frequency earthquakes in back- ground seismicity along subduction zone of South-Western Japan. Eos Trans. 84 (46).

Jet Propulsion Laboratory, 2017. GNSS-inferred positioning system and orbit analysis simulation software (GIPSY-OASIS). Retrieved from. https://gipsy-oasis.jpl.nasa.gov.

Johanson, I.A., Bürgmann, R., 2010. Coseismic and postseismic slip from the 2003 San Simeon earthquake and their effects on backthrust slip and the 2004 Parkfield earthquake. J. Geophys. Res. 115, (B07411), doi:10.1029/2009JB006599.

Klein, E., Duputel, Z., Zigone, D., Vigny, C., Boy, J.P., Doubre, C., Meneses, G., 2018. (2018), Deep Transient Slow Slip Detected by Survey GPS in the Region of Atacama, Chile. Geophys. Res. Lett. 45 (22), 12263–12273. https://doi.org/10.1029/2018GL080613.

Kostoglodov, V., Singh, S.K., Santiago, J.A., Franco, S.I., Larson, K.M., et al., 2003. A large silent earthquake in the Guerrero seismic gap, Mexico. Geophys. Res. Lett. 30, 1807.

Loveless, J.P., Meade, B.J., 2011. Spatial correlation of interseismic coupling and coseismic rupture extent of the 2011 MW = 9.0 Tohoku-oki earthquake. Geophys. Res. Lett. 38 (17), L17306 https://doi.org/10.1029/2011gl048561.

Marone, C., Scholz, C.H., Bilham, R., 1991. On the mechanics of earthquake afterslip. J. Geophys. Res. 96, 8441–8452.

Meade, B.J., 2007. Algorithms for the calculation of exact displacements, strains, and stresses for triangular dislocation elements in a uniform elastic half space. Comput. Geosci. 33, 1064–1075.

Minson, S.E., Simons, M., Beck, J.L., 2013. Bayesian inversion for finite fault earthquake source models I— theory and algorithm. Geophys. J. Int. 194, 1701–1726.

Miyazawa, M., Mori, J., 2005. Detection of triggered deep low fre-quency events from the 2003 Tokachi-oki earthquake. Geophys. Res.Lett. 32, L10307 https://doi.org/10.1029/2005GL022539.

Miyazawa, M., Mori, J., 2006. Evidence suggestingfluidflow beneath Japan due to periodic seismic triggering from the 2004 Sumatra- Andaman earthquake. Geophys. Res. Lett. 33, L05303 https://doi.org/10.1029/2005GL025087.

Mouslopoulou, V., Bocchini, G.-M., Cesca, S., Saltogianni, V., Bedford, J., Petersen, G., Gianniou, M., Oncken, O., 2020. Earthquake-swarms, slow-slip and fault-interactions at the western-end of the Hellenic Subduction System precede the Mw 6.9 Zakynthos

Earthquake, Greece. Geochem. Geophys. Geosyst. 21 (12) https://doi.org/10.1029/2020GC009243 e2020GC009243.
Nijholt, N., et al., 2024. Supporting Information for the Article "Triggered and Recurrent Slow Slip in North Sulawesi, Indonesia". 4TU. Researchdata, doi:10.421/21310383.
Nijholt, N., Simons, W.J.F., Efendi, J., Sarsito, D.A., Riva, R.E.M., 2021. A transient in surface motions dominated by deep afterslip subsequent to a shallow supershear earthquake: the 2018 Mw 7.5 Palu case. Geochem. Geophys. Geosyst. 22 e2020GC009491.
Obara, K., Kato, A., 2016. Connecting slow earthquakes to huge earthquakes. Science 353, 253–257.
Obara, K., et al., 2004. Episodic slow slip events accompanied by non- volcanic tremors in Southwest Japan subduction zone. Geophys. Res. Lett. 31, L23602 https://doi.org/10.1029/2004GL020848.
Okada, Y., 1992. Internal deformation due to shear and tensile faults in a half-space. Bull. Seismol. Soc. Am. 82 (2), 1018–1040.
Outerbridge, K.C., Dixon, T.H., Schwartz, S.Y., Walter, J.I., Protti, M., Gonzalez, V., Biggs, J., Thorwart, M., Rabbel, W., 2010. A tremor and slip event on the Cocos-Caribbean subduction zone as measured by a global positioning system (GPS) and seismic network on the Nicoya Peninsula, Costa Rica. J. Geophys. Res. 115, B10408 https://doi.org/10.1029/2009JB006845.
Ozawa, S., Murakami, M., Kaidzu, M., Tada, T., Sagiya, T., Hatanaka, Y., Yarai, H., Nishimura, T., 2002. Detection and monitoring of ongoing Aseismic slip in the Tokai Region, Central Japan. Science 298, 1009–1012. https://doi.org/10.1126/science.1076780.
Pelinovsky, E., Yuliadi, D., Prasetya, G., et al., 1997. The 1996 Sulawesi Tsunami. Nat. Hazards 16, 29–38.
Radiguet, M., Cotton, F., Vergnolle, M., Campillo, M., Walpersdorf, A., Cotte, N., Kostoglodov, V., 2012. Slow slip events and strain accumulation in the Guerrero gap, Mexico. J. Geophys. Res. 117, B04305 https://doi.org/10.1029/2011JB008801.
Rebischung, P., Schmid, R., 2016. IGS14/igs14.atx: a new framework for the IGS products. AGU Fall Meeting, San Francisco, CA.
Rubinstein, J.L., La Rocca, M., Vidale, J.E., Creager, K.C., Wech, A.G., 2008. Tidal modulation of non-volcanic tremor. Science 319, 186–189.
Saltogianni, V., Mouslopoulou, V., Dielforder, A., Bocchini, G.M., Bedford, J., Oncken, O., 2021. Slow slip triggers the 2018 Mw 6.9 Zakynthos Earthquake within the weakly locked Hellenic Subduction System, Greece. Geochem. Geophys. Geosyst. 22, e2021GC010090 https://doi.org/10.1029/2021GC010090.
Segall, P.A., Bradley, M., 2012. Slow-slip evolves into megathrust earthquakes in 2D numerical simulations. Geophys. Res. Lett. 39, L18308.
Simons, W., Broerse, T., Kleptsova, O., Nijholt, N., Hooper, A., Pietrzak, J., Morishita, Y., Naeije, M., Lhermitte, S., Herman, M., Sarsito, D.A., Efendi, J., Sofian, Govers, R., Vigny, C., Abidian, H.A., Pramono, G.H., Nugroho, C., Visser, P., Riva, R., 2022. A tsunami generated by a strike-slip event: constraints from GPS and SAR data on the 2018 Palu earthquake. J. Geophys. Res. Solid Earth 127, e2022JB024191. https://doi.org/10.1029/2022JB024191.
Simons, W.J.F., Naeije, M.C., Brown, B.E., Niemnil, S., Pradit, S., Thongtham, N., Mustafar, M.A., Towatana, P., Darnsawasdi, R., Yucharoen, M., et al., 2019. Vertical Motion of Phuket Island (1994–2018) due to the Sumatra-Andaman Mega-Thrust Earthquake Cycle: impact on sea-level and consequences for Coral Reefs. Mar. Geol. 414, 92–102. https://doi.org/10.1016/j.margeo.2019.05.008.
Socquet, A., Simons, W., Vigny, C., McCaffrey, R., Subarya, C., Sarsito, D., Ambrosius, B., Spakman, W., 2006. Microblock rotations and fault coupling in SE Asia triple junction (Sulawesi, Indonesia) from GPS and earthquake slip vector data. J. Geophys. Res. Solid Earth 111 (B8).
Socquet, A., Hollingsworth, J., Pathier, E., Bouchon, M., 2019. Evidence of supershear during the 2018 magnitude 7.5 Palu earthquake from space geodesy. Nat. Geosci. 12 (3), 192.
Supendi, P., Nugraha, A.D., Widiyantoro, S., Pesicek, J.D., Thurber, C.H., Abdullah, C.I., et al., 2020. Relocated aftershocks and back- ground seismicity in eastern Indonesia shed light on the 2018 Lombok and Palu earthquake sequences. Geophys. J. Intern. 221 (3), 1845–1855. https://doi.org/10.1093/gji/ggaa118.
Takagi, R., Uchida, N., Obara, K., 2019. Along-strike variation and migration of long-term slow slip events in the western Nankai subduction zone, Japan. J. Geophys. Res. Solid Earth 124, 3853–3880. https://doi.org/10.1029/2018JB016738.
Tarantola, A., 2005. Inverse Problem Theory and Methods for Model Parameter Estimation. SIAM.
Toda, S., Stein, R.S., Reasenberg, P.A., Dieterich, J.H., Yoshida, A., 1998. Stress transferred by the 1995 $M_W = 6.9$ Kobe, Japan, shock: effect on aftershocks and future earthquake probabilities. J. Geophys. Res. 103, 24,543–24,565.
Vigny, C., Perfettini, H., Walpersdorf, A., Lemoine, A., Simons, W., van Loon, D., Bock, Y., 2002. Migration of seismicity and earthquake interactions monitored by GPS in SE Asia triple junction: Sulawesi, Indonesia. J. Geophys. Res. Solid Earth 107 (B10), ETG-7.
Voss, N., Dixon, T.H., Liu, Z., Malservisi, R., Protti, M., Schwartz, S., 2018. Do slow slip events trigger large and great megathrust earthquakes? Sci. Adv. 4, eaat8472.
Wallace, L.M., 2020. Slow slip events in New Zealand. Annu. Rev. Earth Planet. Sci. 48, 175–203. https://doi.org/10.1146/annurev-earth-071719-055104.
Wallace, L.M., Beavan, J., 2010. Diverse slow slip behavior at the Hikurangi sub- duction margin, New Zealand. J. Geophys. Res. 115, B12402 https://doi.org/10.1029/2010JB007717.
Wallace, L.M., Bartlow, N., Hamling, I., Fry, B., 2014. Quake clamps down on slow slip. Geophys. Res. Lett. 41, 8840–8846. https://doi.org/10.1002/2014GL062367.
Wallace, L.M., Hreinsdóttir, S., Ellis, S., Hamling, I., D'Anastasio, E., Denys, P., 2018. Triggered Slow Slip and Afterslip on the Southern Hikurangi Subduction Zone following the Kaikōura Earthquake. Geophys. Res. Lett. 45 (10), 4710–4718. https://doi.org/10.1002/2018GL077385.
Wallace, L.M., Kaneko, Y., Hreinsdóttir, S., Hamling, I., Peng, Z., Bartlow, N., D'Anastasio, E., Fry, B., 2017. Large-scale dynamic triggering of shallow slow slip enhanced by overlying sedimentary wedge. Nat. Geosc. 10 https://doi.org/10.1038/NGEO3021.
Walpersdorf, A., Vigny, C., Subarya, C., Manurung, P., 1998. Monitoring of the Palu-Koro Fault (Sulawesi) by GPS. Geophys. Res. Lett. 25 (13), 2313–2316.
Wei, M., Kaneko, Y., Shi, P., Liu, Y., 2018. Numerical modeling of dynamically triggered shallow slow slip events in New Zealand by the 2016 Mw 7.8 Kaikoura Earthquake. Geophys. Res. Lett. 45 (10), 4764–4772. https://doi.org/10.1029/2018GL077879.